Crystallization Kinetics of PE-*b-isotactic* PMMA Diblock Copolymer Synthesized Using $SiMe_2(Ind)_2ZrMe_2$ and MAO Cocatalyst

Muhammad Atiqullah
King Abdullah University of Science & Technology (KAUST) Center-in-Development for Transformative Research in Petrochemicals and Polymers, King Fahd University of Petroleum & Minerals, Dhahran 31261, Saudi Arabia

Center of Research Excellence in Petroleum Refining and Petrochemicals, King Fahd University of Petroleum & Minerals, Dhahran 31261, Saudi Arabia

Mohammad M. Hossain, Muhammad S. Kamal, Mamdouh A. Al-Harthi, and Masiullah J. Khan
Dept. of Chemical Engineering, King Fahd University of Petroleum & Minerals, Dhahran 31261, Saudi Arabia

Anwar Hossaen and Ikram Hussain
Center for Refining and Petrochemicals, Research Institute, King Fahd University of Petroleum & Minerals, Dhahran 31261, Saudi Arabia

DOI 10.1002/aic.13806

Polyethylene-b-poly(methyl methacrylate) (PE-b-*PMMA) diblock copolymer has important interfacial applications. Hence, a PE*-b-*isotactic PMMA diblock copolymer was synthesized using $SiMe_2(Ind)_2ZrMe_2$ and MAO cocatalyst. The polymerization mechanism and the origin of PMMA isotacticity were duly explained. An appropriate nonisothermal Avrami-Erofeev crystallization model was developed to compare the crystallization kinetics of the above copolymer with that of a PE homopolymer. For both polymers, the model well matched the entire differential scanning calorimeter crystallinity profile, notably for a single Avrami-Erofeev index, and predicted cylindrical crystal growth. This model particularly overcomes the limitations of the published nonisothermal crystallization models, and provides interesting insight into PE crystallization. The PMMA block significantly decreased the heats of crystallization and fusion, % crystallinity, and the relative crystallization function; increased the nonisothermal crystallization rate constant; and introduced minimal dilution effect whereas the PE block formed a continuous or percolated phase. This study correlates catalyst structure, copolymer block tacticity, and PE nonisothermal crystallization and melting behavior.* © 2012 American Institute of Chemical Engineers *AIChE J,* 59: 200–214, 2013

*Keywords: zirconocene catalyst, polyethylene-b-*poly(*methyl methacraylate) diblock copolymer, polymerization mechanism, Avrami-Erofeev equation, nonisothermal crystallization kinetics, differential scanning calorimeter*

Introduction

Polyethylene (PE) backbone does not have a functional moiety. This limits applications that require adhesion, dyability, pronounced surface effects, grafting, and compatibility with other materials. Therefore, PEs, with functional block and graft structures, are synthesized to overcome this limitation.[1–6] In particular, the diblock copolymer of ethylene and methyl methacrylate (a polar ester) (PE-*b*-polymethyl methacrylate [PMMA]) is an important compatibilizer,[7] and it greatly enhances dyability.[1,8,9]

The crystallization study of PE-*b*-stereoPMMA diblock copolymers and the PE homopolymers is theoretically as well as practically important. The crystallization within the block copolymer microdomains, which can introduce interesting morphologies on microscale and nanoscale, is particularly significant from the theoretical viewpoint. Such morphologies originate from the capability of the copolymer blocks to self-organize and separate into microphases. Consequently, block copolymers show attractive properties. Several excellent reviews on block copolymer crystallization are available in the literature.[10–12] The practical importance arises from the pronounced effect of crystallinity and morphology on the physical and chemical properties of PEs.

PE-*b*-stereoPMMA diblock copolymers have semicrystalline PE ‘‘hard block’’ and glassy (amorphous) PMMA ‘‘soft block.’’ The crystallization temperatures of PEs vary from 118 to 125°C.[13–15] On the other hand, the glass transition temperature, for example, of an ‘‘isotactic’’ PMMA ranges from 53 to 58°C.[16,17] This shows that the PE crystallization temperatures are much greater than the PMMA glass transition temperatures. This is an example of soft confinement

---

Correspondence concerning this article should be addressed to M. Atiqullah at matiq@kfupm.edu.sa.

that may result from the glassy PMMA domains or segregation between domains.[11,18] Hence, to study the influence of the methyl methacrylate (MMA) functional soft block on the crystallization kinetics (using model and experiment) is particularly interesting. However, to the best of our knowledge, this has not yet been reported. In this study, we shall use the nonisothermal (constant cooling rate) differential scanning calorimetric (DSC) experiments because they have the following advantages over the isothermal crystallization experiments:[19–22]

- Nonisothermal DSC experiments are fairly fast and simple. They have broader temperature ranges (usually 30.0−35.0°C) (from beginning to completion of crystallization). They detect phase transformations that occur too rapidly to be observed in isothermal experiments. They better approximate the industrial fabrication processes (such as extrusion, injection molding, and film blowing) that are also dynamic and nonisothermal.
- By contrast, isothermal DSC experiments are slower and less convenient. Here, the experimental temperature range (from beginning to completion of crystallization) is narrow (usually 2.0−3.0°C). The base line is difficult to accurately determine. The sample needs to be heated to the desired temperature in a time that is much smaller than the crystallization time. Isothermal measurements are only possible when the thermal response time of the measured polymer is smaller than the rate of the crystallization process.

In the literature, the following nonisothermal crystallization models are available. They were developed by Jeziorny,[23] Ozawa,[21] and Liu et al.[24] However, these models have several limitations, which we discuss below.

Jeziorny[23] introduced the effect of constant DSC cooling rate β on crystallization kinetics by converting the Avrami-Erofeev isothermal crystallization rate constant k to the corresponding nonisothermal analogue $k'(T)$, using the expression $\ln k'(T) = \frac{\ln k}{\beta}$. This was so done assuming that the rate of crystallization obeys the following first-order relation[23]

$$\frac{d\alpha(T)}{dt} = k'(T) \times (1 - \alpha(T)) \tag{1}$$

where $\alpha(T)$ is the temperature-dependent relative crystallinity (degree of crystallization) and t is the time of crystallization.

The Jeziorny model has the following limitations. First, Eq. 1, hence the above assumption, contradicts with the phenomenological development of the nonisothermal Avrami-Erofeev crystallization rate expression. See the development of our rigorous crystallization model and Appendix A for the details. Also, note that the division of ln k by β (a constant term) does not make it temperature-dependent for a constant cooling rate experiment. Second, the double logarithmic plot of $\ln[-\ln(1 - \alpha(t))]$ vs. $\ln t$, used to determine the Avrami-Erofeev index n, is fairly insensitive to its argument.[23]

Ozawa's treatment uses multiple constant cooling rate DSC experiments; it cannot model a single cooling rate nonisothermal crystallization experiment. Here, $\ln[-\ln(1 - \alpha(T))]$ vs. cooling rate β is plotted to determine the crystallization kinetic parameters. The dependent variable $\ln[-\ln(1 - \alpha(T))]$ is generated by selecting $\alpha(T)$s corresponding to the same value of T in the different constant cooling rate crystallization profiles. This means that T is used as the parametric variable. The problem of double logarithmic insensitivity also exists here.[21]

The relative crystallinity depends on β, t, and T. Therefore, Liu et al.[24] combined the treatment of Avrami with that of Ozawa as follows

$$\ln \beta = \ln F(T) - b \ln t \tag{2}$$

where $F(T) = \left[\frac{k^*(T)}{k}\right]^{\frac{1}{m}}$ refers to the cooling rate required to attain a defined relative crystallinity in a given time; m is the Ozawa index; b is the ratio of Avrami to Ozawa indices. The plot of ln β vs. ln t, as per Eq. 2, gives a straight line. The intercept and slope give $F(T)$ and b, respectively. The independent variable ln t is generated by selecting ts corresponding to the same value of relative crystallinity in the different constant cooling rate crystallization profiles. Therefore, relative crystallinity serves as the parametric variable. The limitations of Avrami-Ozawa hybrid model are as follows. The index b, being an empirical parameter, does not indicate the crystal growth dimension n even though it may be used to selectively fit to the acquired DSC crystallization data. A single cooling rate experiment is as well inapplicable in this case.

All the above three nonisothermal models use the logarithmic linearization approach. This is a common data handling flaw. Also, they do not thoroughly apply to the entire crystallization profile; limited data points, usually in the linear region, are used to arbitrarily draw the straight line. Moreover, these models cannot determine the apparent activation energy of crystallization. Hence, we conclude that a rigorous appropriate nonisothermal polymer crystallization model that applies to the entire single cooling rate experiment be developed.

To study the crystallization kinetics, the route to synthesize PE-*b*-stereoPMMA diblock copolymers should be judiciously selected. In this regard, we would like to remark that metallocenes generally catalyze the sequential copolymerization of MMA with an olefin that produces linear polyolefin without short-chain branches.[25,26] They can, in particular, separately homopolymerize ethylene and MMA. Also, because of versatile organometallic structures, they can immensely vary the stereoregularity of the PMMA block. Thus, they represent an important industrial and applied catalysis research topic.

In view of the previous discussion, this study was organized as follows:

1. Synthesize the PE-*b*-PMMA diblock copolymer, the ethylene homopolymer, and PMMA using $SiMe_2(Ind)_2ZrMe_2$ and the MAO (methylaluminoxane) cocatalyst; and elucidate the progression in polymerization mechanism.
2. Develop a rigorous and versatile nonisothermal PE crystallization model that has the following characteristics:
   1. It well matches the entire single cooling rate crystallization profile, and accordingly better illustrates the crystallization mechanism than do the alternative models.
   2. It calculates the crystallization kinetic parameters (i.e., the frequency factor, apparent activation energy, and crystal growth dimension with confinement) and relative crystallization function from a single cooling rate DSC experiment.
   3. It illustrates the role of PE backbone microstructure in polymer crystallization (including the major

thermal properties) in a more phenomenological fashion in order that the crystallization kinetics and melting behavior of the PE-*b*-PMMA diblock copolymer can be compared with those of the reference ethylene homopolymer.

3. Model the lamellar thickness distributions of the crystallized PEs, using Gibbs-Thomson equation[27–30] and DSC experiments. This enables us to learn about the topological constraint of the polymer chains and post-crystallization status of the polymer crystallite matrix from a nanoscopic view point.

Experimental Section

Materials

$Me_2Si(Ind)_2ZrMe_2$ and MAO (10 wt % in toluene) were purchased from MetCat and Chemtura, Germany, respectively. Analytical grade triisobutylaluminum (TIBA) (2 M in heptane), toluene, *n*-hexane (both 99.999% pure), A4 molecular sieve, 2,6-di-*tert*-butyl-4-methyl phenol (BHT), MMA, basic alumina, 1,2,4 trichlorobenzene (TCB), toluene-d_6, and 1,2 dichlorobenzene-d_4–all were obtained from Sigma-Aldrich. Ethylene and argon (99.999% pure) were procured from Abdullah Hasim, a local vendor.

Synthesis of polymers

PMMA: The synthesis of PMMA requires that the monomer should be extremely pure to prevent the catalyst from getting poisoned by any impurity. Therefore, we first purified the methylmethacraylate (MMA) monomer as follows.

The as-received MMA contains hydroquinone inhibitor and moisture. This inhibitor was removed using the following steps. MMA was passed drop by drop through a chromatographic column (three-quarter filled with basic alumina). This was done twice, and each pass took about 40 min. Then, the alumina-treated MMA was vacuum distilled at 60°C under 90 mm Hg of pressure. The moisture content of this distilled MMA was determined to be about 450 ppm. A Mettler DL37 KF Coulometer was used to reduce this high moisture level to $\leq$10 ppm by contacting the MMA with 4A molecular sieve under bubbling of argon.

Next, we purified toluene as follows. It was first dried over night using 4A molecular sieve; then it was evacuated and purged with argon several times. This procedure reduced the moisture level to $\leq$10 ppm. Following the purification of MMA and drying of toluene, we polymerized this monomer using $Me_2Si(Ind)_2ZrMe_2$ and MAO as summarized below.

A thick-walled 250 mL Imtech glass reactor was baked at about 150°C to remove the moisture sticking to its inner wall. It was then cooled to room-temperature and closed using the top lid. At this stage, the reactor was evacuated and purged with argon several times. About 15 mL toluene and 0.1 mL TIBA were introduced into the reactor. The resulting mixture was stirred for 10 min using a magnetic stirrer. TIBA was used as the scavenger. A 4 mL solution of the catalyst [$Me_2Si(Ind)_2ZrMe_2$, 4 μmol/(mL of toluene)] was prepared in the dried toluene and added to the reactor. Then, the cocatalyst—0.1 mL 10 wt % MAO—was fed to the reactor. After 10 min, 3 mL purified MMA was added to start the polymerization under argon, which was continued for 90 min at room-temperature. The polymerization was quenched by adding acidic methanol. The resulting PMMA was precipitated using excess methanol. The product was washed thrice using methanol and dried over night. The yield was 2.650 g.

Ethylene Homopolymer: The baked reactor was fed with the same volume of dried toluene, TMA scavenger, $Me_2Si(Ind)_2ZrMe_2$, and MAO as used for MMA polymerization. $Me_2Si(Ind)_2ZrMe_2$ concentration was also kept the same. Then ethylene, passing through moisture and oxygen scavenging columns (one each), fed the reactor at 2 bar(g). The polymerization was continued for 15 min; then it was quenched; and the product was separated, washed, and dried applying the method used during the synthesis of PMMA. The polymer yield was 0.350 g.

PE-b-MMA Diblock Copolymer: MMA was copolymerized with ethylene following the same procedures and reaction conditions applied to synthesize PMMA and ethylene homopolymer. However, the following steps varied. MMA was introduced sequentially after feeding of ethylene for 15 min. The total polymerization run time was 60 min. The polymer yield was 0.500 g.

Thermal properties

The thermal properties of the synthesized PEs were measured in terms of peak melting temperature (T_{pm}), peak crystallization temperature (T_{pc}), and % crystallinity, using a DSC (DSC Q2000, Texas Instruments). The instrument was calibrated using indium.

About 4.0 mg of the sample was taken in an aluminum pan, which was tightly closed with a lid. A sealed aluminum pan (without the sample) was used as a reference. The polymer samples and the reference were placed in the instrument carrousel. The synthesized polymer samples were heated at 10°C/min from room-temperature to 160°C, using a nitrogen flow rate of 50 mL/min. This is called Cycle 1. After this, they were isothermally heated for 5 min to remove the influence of the thermal history and unmelted crystals that could cause heterogeneous cystallization. Next, they were cooled from 160°C to room-temperature using the above thermal ramp value, and were kept at this temperature for 5 min. This is Cycle 2. Finally, the samples were reheated at 10°C/min to 160°C (Cycle 3).

The peak melting temperature (T_{pm}) and the % crystallinity were determined from Cycle 3. The thermogram under Cycle 3 endotherm was integrated to measure the heat of fusion (H_f), which is proportional to the crystallinity of the polymer. The % crystallinity was calculated from $\frac{\Delta H_f^0 (J/g)}{\Delta H_{std}^0 (J/g)}$ where $\Delta H_{std} = 290.0$ J/g is the heat of fusion of a perfectly crystalline PE.[31,32] The peak crystallization temperature (T_{pc}) was determined from the Cycle 2 crystallization exotherm. The data for each cycle were acquired and analyzed using the TA explorer software.

The glass transition temperature T_g of the synthesized PMMA was determined using Cycle 3. However, here a heating rate of 20°C/min was used. T_g was estimated as the temperature at the midpoint of the line drawn between (1) the temperature of intersection of the initial tangent with the tangent drawn through the point of inflection of the DSC thermogram and (2) the temperature of intersection of the tangent drawn through the point of inflection with the final tangent.

The lamellar thickness distribution was determined using the constant heating rate DSC experiment. The mathematical treatment for this is provided in Appendix B.

Table 1. Properties of the Synthesized Polymers

Polymer Characteristics	PE Homopolymer	PE_{50}-*b*-$PMMA_{50}$ Diblock Copolymer	Isotactic PMMA
Weight average molecular weight (g/mol)	85,785*	181,732[†]	294,563[†]
PDI	2.50	2.60	2.10
Average copolymer composition (mol % MMA)	None	22.0	MMA homopolymer
Average copolymer composition (wt % MMA)	None	50.0	MMA homopolymer
Peak melting (T_{pm}) (°C)	132.4	131.2	◆
Peak crystallization point (T_{pc}) (°C)	116.4	115.9	◆
Temperature for maximum nonisothermal relative crystallinity function (°C)	117.0[‡]	114.0[‡]	Not applicable
Glass transition temperature (°C)	Semicrystalline polymer	Semicrystalline polymer	55.10
Heat of crystallization ΔH_c (J/g)	210.60	216.40,[§] 108.20[¶]	◆
Heat of fusion ΔH_f (J/g)	214.80	107.40,[§] 213.94[¶]	◆
% Crystallinity	74.08	37.03,[§] 73.77[¶]	◆
Most probable lamellar thickness (nm)	9.45**	9.12**	Not applicable

*Based on polystyrene-PE Mark-Houwink constants.
[†] Relative to polystyrene standards.
[‡] Determined from Figure 8.
[§] With respect to the total mass of the copolymer.
[¶] With respect to the mass of the PE block.
**Estimated from Figure 9.
◆No transformation was noted in the DSC thermogram.

Average molecular weight and polydispersity index

The synthesized ethylene homopolymer, PE-*b*-PMMA diblock copolymer, and PMMA were characterized in terms of molecular properties (weight average molecular weight and polydispersity index [PDI]) using gel permeation chromatography (GPC; Polymer Lab GPC 220, UK). PLgel 10 μm mixed-B column was used. The column temperature was kept constant at 160°C.

The antioxidant, BHT (0.0125 wt %), was added to TCB (solvent) to prevent the polymer samples from degrading. Then, 2.8 mg of polymer sample was taken in a 1.5 mL vial, and the polymer was dissolved in 1.0 mL stabilized TCB as follows. The polymer-containing sample vials were placed in the warming compartment of the GPC instrument at 90°C for about 1 h. During this period, the vials were shaken every 15 min to completely dissolve the polymers.

Before injecting the samples, the differential refractive index detector was purged for 4 h using TCB (1 mL/min) to get a stable baseline. Also, the inlet pressure portal and the differential pressure output were purged for 1 h.

The sample injection volume and flow rate were 100 μL and 1.0 mL/min, respectively. The instrument was calibrated using nine polystyrene standards whose peak molecular weights ranged from 2,608,000 to 1530 g/mol. The polystyrene calibration curve was converted into the corresponding PE calibration curve using the Mark-Houwink constants of both polymers.[33] The run time for each sample was 20 min. The Cirrus single detector software was used to calculate the average molecular weights and the PDI, which are reported in Table 1.

Copolymer composition distribution

The comonomer composition distribution (CCD) of the experimental sample(s) was determined using a Polymer Char CRYSTAF instrument. This consists of five 50 mL stainless steel stirred crystallization vessels, which are placed in a gas chromatographic oven. These vessels are connected, via a rotary valve, to a dual-channel optoelectronic infrared (IR) detector having 3.5 μm measurement wave length. The sample solutions were prepared and run as follows.

About 5 mg of sample was placed in a crystallization vessel. This was dissolved at 150°C by adding 40 mL of TCB and stirring the mixture for 60 min. The solution was equilibrated at 95°C for 45 min. The temperature of the IR cell was maintained at 150°C. The solution was crystallized by cooling at 0.2°C/min from 95 to 30°C to obtain the desired composition distribution.

Average copolymer composition

The average composition of the PE-*b*-PMMA diblock copolymer, in terms of mol % of MMA, was determined using ^{1}H NMR (nuclear magnetic resonance) spectroscopy. For this purpose, a Jeol 500 MHz instrument was used. The experimental sample solution was prepared by dissolving about 10 mg of the polymer sample in about 0.5 mL of TCB at 130°C, using a 5 mm NMR tube. Finally, 0.5 mL 1,2-dichlorobenzene-d_4 was added to the NMR tube. The sample vial was shaken using a high-temperature sample preparation instrument (PL-SP 260), and the temperature was increased from room-temperature using a ramp of 10°C/min.

Deuterated benzene-d_6 was used as the internal standard to get the lock. The spectral data were acquired (applying standard parameters for proton) and processed using the WIN LAMBDA software. Table 2 lists the NMR experimental conditions. For the NMR assay of PMMA, deuterated chloroform was used as the solvent.

Development of rigorous crystallization model

The development of the target rigorous nonisothermal crystallization model is based on the extension of the isothermal Avrami-Erofeev crystallization rate equation to the nonisothermal situation. Appendix A details the derivation of the isothermal crystallization rate equation.

Table 2. Operating Conditions of the NMR Spectrometer

Acquired Data Points	Data Acquisition Time (s)	Scan Number	Spectral Width (HZ)	Pulse Width (μs)	Flip Angle (°)	Pulse Delay (s)	Probe Temperature (°C)
32,000	3.28	8	10,000	6	45	6.18	100

For the nonisothermal case, we first assume the following:

1. The nucleation and growth rates depend only on temperature. They are proportional to each other, and have the same temperature dependence—very often an Arrhenius behavior.[19,34] Hence, they are "isokinetic," which applies because the polymer crystallization, in this particular case, can be reversed from solid to the molten state on heating at the same rate. Note that Avrami's rigorous treatment was not restricted to isothermal conditions; it was originally derived for the isokinetic case.[35]

2. A nonisothermal crystallization can be expressed as the superposition of a sequence of small isothermal crystallization steps.[36]

3. The crystallization rate depends only on the state variables α and T, and not on the thermal history (heating rates).[19,37,38]

4. The crystallization products and mechanism do not change with temperature.[39]

According to Assumption 1, the crystal growth rate constant k_{grow}, and the nucleation rate constant k_{nucl} can be, respectively, written as follows[40–42]

$$k_{\mathrm{grow}} = k_{\mathrm{grow},0} \exp\left[\frac{-E_{\mathrm{grow}}}{R}\left(\frac{1}{T} - \frac{1}{T_0}\right)\right] \tag{3}$$

$$k_{\mathrm{nucl}} = k_{\mathrm{nucl},0} \exp\left[\frac{-E_{\mathrm{nucl}}}{R}\left(\frac{1}{T} - \frac{1}{T_0}\right)\right] \tag{4}$$

where $k_{\mathrm{grow},0}$ and E_{grow} are the frequency factor and activation energy of crystal growth, respectively. $K_{\mathrm{nucl},0}$ and E_{nucl} represent the corresponding terms for nucleation, respectively. T is the absolute temperature of the crystallizing polymer at any time t. T_0 is the centering temperature. R is the universal gas constant. Note that the above type of Arrhenius relation suits the numerical treatment of a typical sigmoidal relative crystallinity vs. T curve.[35] Additionally, the centering procedure facilitates searching the kinetic parameters by minimizing the statistical correlation between activation energy and pre-exponential factor.[42–44]

Using Eqs. 3, 4, and A12, the overall nonisothermal crystallization rate constant $k'(T)$ can be expressed as

$$k'(T) = \left[\frac{K_s N_0}{V_0}\right]\frac{k_{\mathrm{grow},0}}{k_{\mathrm{nucl},0}} \times \exp\left[-\frac{(E_{\mathrm{grow}} - E_{\mathrm{nucl}})}{R}\left(\frac{1}{T} - \frac{1}{T_0}\right)\right] \tag{5}$$

Putting $k_0 = \left[\frac{K_s N_0}{V_0}\right]\frac{k_{\mathrm{grow},0}}{k_{\mathrm{nucl},0}}$ (overall crystallization frequency factor), and (E_{grow}−E_{nucl}) = E_a (apparent crystallization activation energy), we can write

$$k\prime(T) = k_0 \times \exp\left[-\frac{E_a}{R}\left(\frac{1}{T} - \frac{1}{T_0}\right)\right] \tag{6}$$

As per Assumptions 2 to 4, Eq. A18 will represent the "isothermal" Avrami-Erofeev relative crystallinity function as follows

$$f(\alpha) = n(1-\alpha)\,[-\ln(1-\alpha)]^{\frac{n-1}{n}} \tag{7}$$

Therefore, the "nonisothermal" Avrami-Erofeev polymer crystallization rate, according to Eqs. A17 and 7, can be written as

$$\frac{d\alpha}{dt} = k_0 \times \exp\left[-\frac{E_a}{R}\left(\frac{1}{T} - \frac{1}{T_0}\right)\right] \times n(1-\alpha)\,[-\ln(1-\alpha)]^{\frac{n-1}{n}} \tag{8}$$

For a given volume of polymer, being crystallized in a DSC using a constant cooling rate $\frac{dT}{dt} = \beta$, Eq. 8 can be finally expressed as

$$\frac{d\alpha}{dT} = \frac{k_0}{\beta} \times \exp\left[-\frac{E_a}{R}\left(\frac{1}{T} - \frac{1}{T_0}\right)\right] \times n(1-\alpha)\,[-\ln(1-\alpha)]^{\frac{n-1}{n}} \tag{9}$$

The above mathematical treatment shows how Eq. 9 has been developed under a set of phenomenological assumptions. Note the following special features of Eq. 9:

- It is a kinetic equation and abides by the laws of conservation of mass and energy.
- The kinetic parameters k_0, E_a, and n can be obtained from a single constant cooling rate DSC trial.
- The interdependence among k_0, E_a, and n can be determined using the statistical cross-correlation coefficient.
- New insight concerning the effect of polymer microstructure on crystallization can be obtained by plotting $f(\alpha)$ as a function of α and $\frac{1}{T}$.

α is related to the corresponding weight fraction relative crystallinity α_w through Eq. 8[45]

$$\alpha = \frac{\alpha_w}{\alpha_w + (\rho_c/\rho_a)\,[1 - \alpha_w]} \tag{10}$$

where ρ_c and ρ_a are the densities of the crystalline and amorphous phases, respectively. For PE, $\rho_c = 1.004$ and $\rho_a = 0.853$.

α_w can be calculated from a typical constant cooling rate DSC experiment using Eq. 11

$$\alpha_w = \frac{\Delta H(T)}{\Delta H_{\mathrm{total}}} = \frac{\int_{T_0}^{T}\left(\frac{dH}{dT}\right)dT}{\int_{T_0}^{T_\infty}\left(\frac{dH}{dT}\right)dT} \tag{11}$$

where $\Delta H_{\mathrm{total}}$ is the maximum enthalpy value reached at the end of the nonisothermal crystallization process and $\Delta H(T)$ is the enthalpy evolved as a function of crystallization temperature T. T_0 and T_∞ represent the start and completion temperatures of crystallization, respectively. $\Delta H_{\mathrm{total}}$ and $\Delta H(T)$ both can be acquired using the software of a standard DSC.

Using Eq. 10, the DSC-generated α_w can be converted to the corresponding volume fraction α. Therefore, we can now solve Eq. 9 numerically using the experimental α_w.

Numerical solution of model equation and kinetic parameter estimation

Equation 9, which represents the nonisothermal Avrami-Erofeev polymer crystallization rate, was evaluated by a least square fitting of the model parameters, using the experimental DSC relative crystallinity α_w and the MATLAB *lsqcurvefit* optimization routine. For this purpose, the α_w vs. T data points, generated by the single constant cooling rate DSC experiments, were taken over the entire crystallization profile to provide a global solution to the problem. All the α_ws were converted to the corresponding αs by using Eq. 10.

Table 3. Model-Predicted Nonisothermal Crystallization Kinetic Parameters

Synthesized Polymers	Avrami-Erofeev Index n	Apparent activation energy E_a (kJ/mol)	Frequency factor k_0 (s^{-1})	Coefficient of determination R^2
PE homopolymer	2.26 ± 0.20	37.29 ± 3.69	0.624 ± 0.04	0.990
PE_{50}-*b*-$PMMA_{50}$ diblock copolymer	1.91 ± 0.08	31.28 ± 1.24	0.699 ± 0.01	0.975

The above crystallization rate equation was numerically solved using the fourth-order Runge-Kutta method (MATLAB ODE 45). During this process, the right hand side was implicitly converted into the temperature integral $\int \exp\left(-\frac{E_a}{RT}\right) dT$, which was subsequently integrated numerically. This method ensures a very high level of accuracy.[46,47] The centering temperature T_0 was taken equal to 370°K that is the arithmetic average of the beginning and final crystallization temperatures. The right hand side of Eq. 9, containing $-\ln(1-\alpha)$, has a point of discontinuity at $\alpha = 1$. This was overcome by approximating $\alpha \cong 0.98$.

The crystallization data, generated by the DSC experiments, were highly reproducible. Repeated experiments were within standard deviations of 1.5% and 3.5% for the PE homopolymer and the block copolymer, respectively. The parameters were determined at 95% confidence limit. In each case, 48 experimental data points were taken for parameter estimation. Thus, for a given value of n, the degree of freedom for the model equals to 45 (number of data points−number of parameters to be estimated = 48−3). This reflects that considerable experimental data were considered to iterate the model parameters. This particular feature makes the model predictions more accurate. Convergence was accepted when the model function changed less than the specified tolerance of 10^{-8}.

The performance of the developed crystallization model (for different values of n) was assessed based on the following:

- coefficient of determination (R^2);
- low sum of the squares of the residuals;
- low cross-correlation coefficient (γ); and
- individual confidence intervals for the model parameters.

As per the above criteria, Table 3 lists the kinetic parameters for the synthesized PEs.

Results and Discussion

We present and discuss the results of this study under the following three subsections:

- Synthesis of polymers: microstructures and mechanisms.
- Developed crystallization model vs. DSC experiments, and significance of model predictions.
- Postcrystallization PE properties.

Synthesis of polymers: microstructure and polymerization mechanism

Figure 1 shows the ^1H NMR (500 MHz) spectrum of the synthesized PMMA. This resembles the typical proton spectrum of an isotactic PMMA having the following characteristic features:[48]

- The presence of the methylene protons following an AB pattern corresponding to $\delta = 1.50-1.53$ ppm and $\delta = 2.12-2.15$ ppm. Here, the methylene protons, unlike those in syndiotactic PMMA, are not magnetically equivalent. Hence, they show a duplet resonance.
- The existence of the —OCH_3 (methoxy)/—$COOCH_3$ (methacrylate) group at $\delta = 3.59$ ppm; and the —CH_3 (methyl) group at $\delta = 1.20$ ppm.

Table 1 reports that the glass transition temperature T_g of the synthesized PMMA is 55.1°C, which matches what has been reported in the literature.[16,17] Therefore, the $Me_2Si(Ind)_2ZrMe_2$/MAO catalyst successfully synthesized an isotactic PMMA.

Figure 2 is the ^1H NMR (500 MHz) spectrum of the synthesized PE-*b*-PMMA diblock copolymer. The presence of

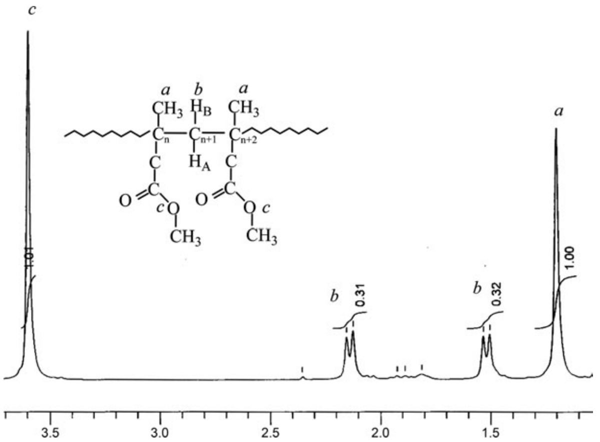

Figure 1. **^1H NMR (500 MHz) spectrogram of the isotactic PMMA synthesized by $Me_2Si(Ind)_2Me_2$/MAO catalyst.**

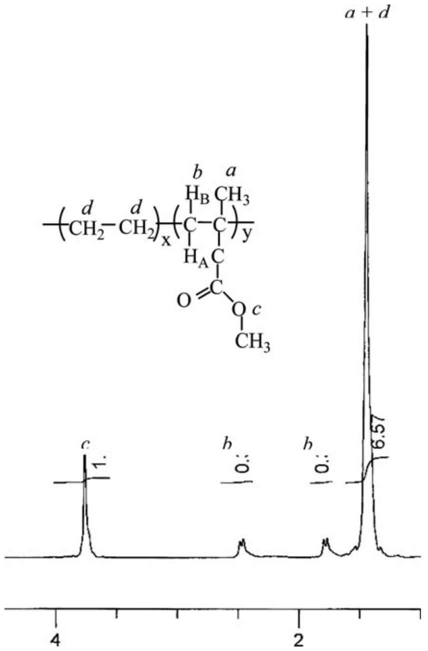

Figure 2. **^1H NMR (500 MHz) spectrogram of the PE-*b*-isotactic PMMA diblock copolymer synthesized by $Me_2Si(Ind)_2Me_2$/MAO catalyst.**

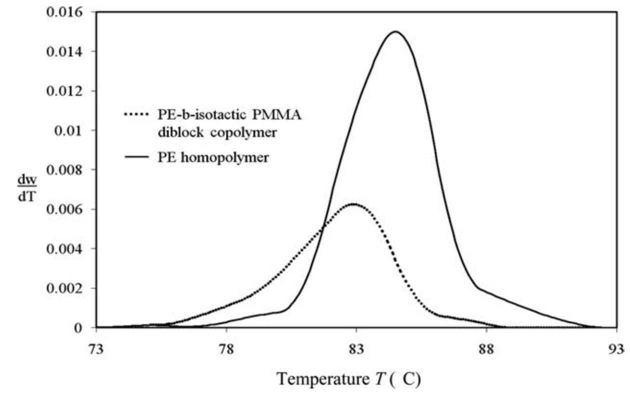

Figure 3. Crystaf analysis of the experimental polymer samples—PE-*b*-isotactic PMMA diblock copolymer vs. PE homopolymer.

the AB type methylene protons and $-OCH_3$/$-COOCH_3$ and $-CH_3$ groups confirm the formation of the isotactic PMMA block. On the other hand, the peak at $\delta = 1.48$ ppm evidences the formation of the PE homopolymer block. However, we would like to comment that such findings by the NMR spectroscopy are only sufficient but not the required proof of the formation of a typical PE_{50}-*b*-isotactic $PMMA_{50}$ diblock copolymer. Note that the subscripts represent the weight percent of each block. See Table 1. This is so because NMR spectroscopy cannot evaluate segregation effects[49–51] that occur in typical copolymerization reactions. For example, Figure 2 would also apply if PMMA and PE homopolymer were independently formed by $Me_2Si(Ind)_2ZrMe_2$ during copolymerization of MMA and ethylene due to complete segregation effects. The required proof, therefore, is to demonstrate that each of the synthesized copolymer backbones comprises PE homopolymer and isotactic PMMA together. Therefore, we determined the composition distribution (CCD) of the synthesized PEs using the crystallization fractionation (Crystaf) technique.[52–55] This is shown in Figure 3.

In Crystaf analysis, the diblock copolymer backbones with lower PMMA content crystallized from the solution at a higher-temperature (during cooling) than the ones with a higher PMMA content. With the progress of crystallization, the sample concentration was continuously monitored. Accordingly, we observe the following in Figure 3. The copolymer Crystaf curve significantly differed in height from that of the PE homopolymer, as well as it drifted toward the left. Also, the σ values, representing the width of the distributions, varied; $\sigma|_{\text{Copolymer Crystaf curve}} = 7.5$; and $\sigma|_{\text{PE homopolymer Crystaf curve}} = 1.3$. Note that the subject block copolymer Crystaf curve would have coincided with that of the reference PE curve if the amorphous PMMA block were absent in the copolymer backbones. However, Figure 3 does not support this. Therefore, we conclude that the PMMA block got incorporated into the growing PE backbones.

Now, we discuss the mechanisms of polymerization with reference to Schemes 1 and 2. We postulated the mechanisms based on the published zirconocene-catalyzed polymerizations of MMA and ethylene in the presence of a Lewis acid cocatalyst. The production of the catalytically active zirconocenium cation[56–63] through the abstraction of the $-CH_3$ ligand by the MAO cocatalyst from $SiMe_2(Ind)_2ZrMe_2$, is the common step in the polymerization of these monomers. First, we summarize the mechanism for

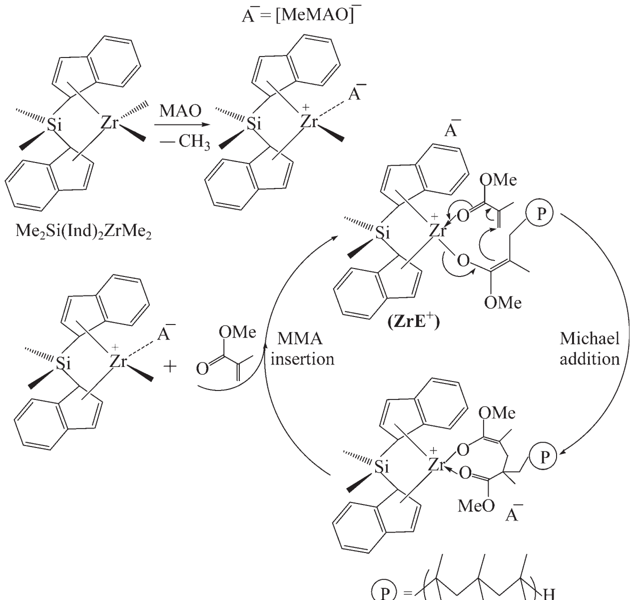

Scheme 1. Mechanism of formation of isotactic PMMA proposed by Höcker et al.,[64] and Delgado and Chen[65].

This is based on the concept of initiation and propagation of polymerization through the cationic zirconocenium ester enolate $[SiMe_2(Ind)_2ZrMe]^{+}$←MMA (ZrE^{+}).

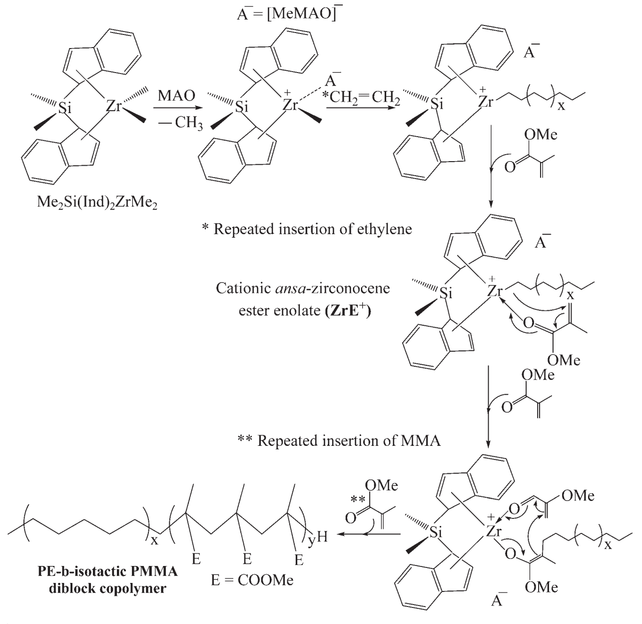

Scheme 2. Mechanism of formation of PE-b-isotactic PMMA diblock copolymer.

The PE block is formed as per the active cationic alkyl zirconocenium $[SiMe_2(Ind)_2ZrMe]^{+}$, following the Cossee-Arlman olefin coordination insertion mechanism[66,67]. The isotactic PMMA block is formed according to Scheme 1.

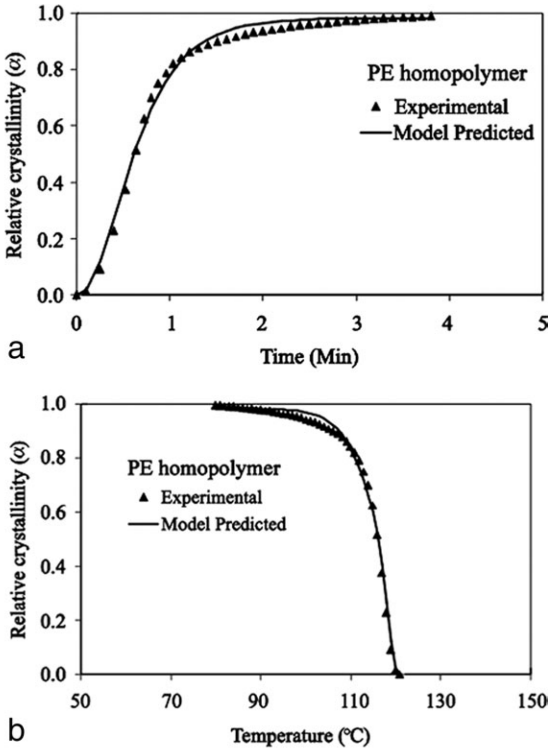

Figure 4. (a) Comparison of model-predicted relative crystallinity with the experimental data as a function of DSC cooling time for PE homopolymer; (b) comparison of model-predicted relative crystallinity with the experimental data as a function of DSC cooling temperature for PE homopolymer.

the isotactic PMMA (Scheme 1); then that for the PE-*b*-isotactic PMMA diblock copolymer (Scheme 2).

According to Scheme 1, the cationic chiral *ansa*-zirconocene ester enolate acts itself as a propagating species for the isospecific polymerization of MMA. The C_2-symmetry of $SiMe_2(Ind)_2ZrMe_2$ introduces isotacticity (with respect to —CH_3 and —COOMe) into the growing PMMA backbone through an enantiomorphic site control mechanism.[64,65] The polymerization proceeds through monometallic intramolecular Michael addition (via cyclic ester enolate intermediate). This means that ZrE^+ activates an incoming MMA molecule as an "acceptor," and the growing chain end as a "donor."

Next, we address the polymerization mechanism for the PE-*b*-isotactic diblock copolymer (Scheme 2). In the sequential synthesis protocol we used, the first step concerns the growth of the PE block through the insertion of ethylene into the C—M bond of the active cationic alkyl zirconocenium $[SiMe_2(Ind)_2ZrMe]^+$, following the well-known Cossee-Arlman olefin coordination insertion mechanism.[66,67] We assume that the used $MAO|_{cocatalyst}$:$SiMe_2(Ind)_2ZrMe_2|_{catalyst}$ molar ratio (Al:Zr = 1:180) converts all the dimethyl zirconocene to the corresponding cationic methyl zirconocenium during the polymerization of ethylene. In the next step, with the addition of MMA, the polymerization activator/initiator shifts from the simple cationic alkyl zirconocenium to the coordinated cationic zirconocene ester enolate (ZrE^+). However, MMA, because of having structural unsaturated carbonyl and (α, β) conjugated alkene, gets inserted into the PE C—M bond through Michael addition. Consequently, the coordinated MMA becomes an integral part of the growing polymer chain. During MMA insertion and chain propagation, the C_2-symmetry of $SiMe_2(Ind)_2ZrMe_2$ imparts isotacticity to the growing PMMA chain through enantiomorphic site control mechanism.[64,65] Therefore, ZrE^+ acts both as an initiator and a propagator for the isotactic PMMA block through repeated Michael addition. This phenomenon is common between MMA homopolymerization and its copolymerization with the growing PE block. What we propose in this regard aligns with the mechanism for isotactic polymerization of MMA (by a cationic chiral *ansa*-zirconocene ester enolate) suggested by Höcker and coworkers[64] and Delgado and Chen et al.[65] (Scheme 1).

Developed crystallization model vs. DSC experiments, and significance of model predictions

Figures 4a, b compare the model-predicted relative crystallinity profile of the PE homopolymer with that of the experimental one as a function of time and temperature, respectively. Figures 5a, b do the same for the PE-*b*-isotactic diblock PMMA copolymer. We observe that for either polymer, the developed rigorous nonisothermal model very well predicts the entire experimental relative crystallinity profile with coefficients of determination $R^2 = 0.990$ and 0.975 for PE homopolymer and PE-*b*-isotactic diblock PMMA copolymer, respectively. Table 3 reports the model-predicted crystallization kinetic parameters (Avrami-Erofeev index n,

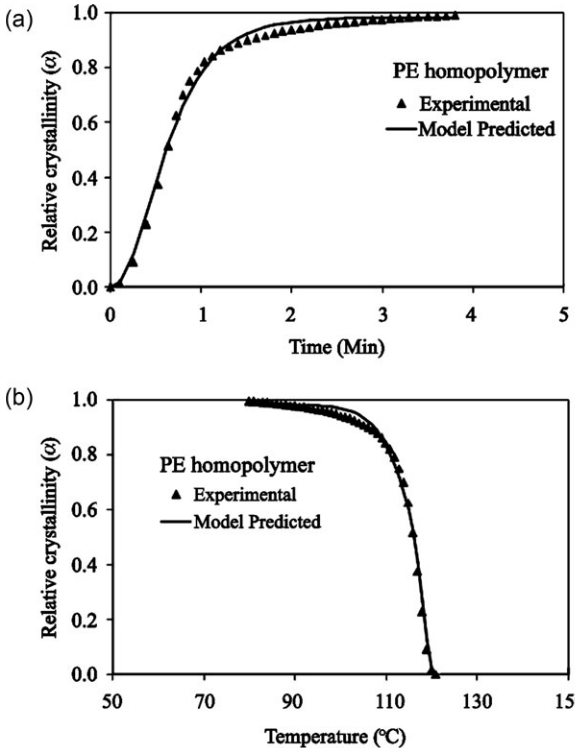

Figure 5. (a) Comparison of model-predicted relative crystallinity with the experimental data as a function of DSC cooling time for PE-*b*-PMMA block copolymer; (b) comparison of model-predicted relative crystallinity with the experimental data as a function of DSC cooling temperature for PE-*b*-PMMA block copolymer.

Table 4. Cross-Correlation Matrix for the Model-Predicted Kinetic Parameters

Synthesized Polymers	Avrami-Erofeev Index n	Apparent Activation Energy E_a	Frequency Factor k_0
PE homopolymer	1.0000	0.7619	0.8435
	0.7619	1.0000	0.8034
	0.8435	0.8034	1.0000
PE_{50}-*b*-$PMMA_{50}$ diblock copolymer	1.0000	0.7457	0.8901
	0.7457	1.0000	0.8502
	0.8901	0.8502	1.0000

apparent activation energy E_a, and crystallization frequency factor k_0) for each polymer. The resulting cross-correlation matrices are reported in Table 4, which indicate a relatively moderate parametric interaction. The linear relationship between ln k' (T) and $\frac{1}{T}$, as shown by Figure 6, ratifies the validity of the Arrhenius form of crystallization rate constant (Eq. 6) for both polymers. Consequently, we conclude that the model-predicted E_a and k_0 are reliable. Also, the isokinetic assumption (related to nucleation and crystal growth) is justified because the polymer crystallization, in this particular case, can be reversed from solid to the molten state upon heating at the same rate. Some relevant examples concerning reversible processes are available in the literature.[42,68]

The important finding, in Figures 4 and 5, is the following. A single value of n represents the whole crystallization regime—primary as well as secondary. This result has great physical significance. This means that the same mechanism of nucleation and crystal growth that we assumed in the development of the constitutive model equation holds all throughout the crystallization process. This evidences how the present model overcomes the drawbacks and limitations of the existing nonisothermal crystallization models. Use of multiple ns, that is, change in crystallization mechanism, as reported in the literature,[69–73] does not appear to be necessary.

Now, we discuss the crystallization behavior of the synthesized PEs categorically with respect to model-predicted n, E_a, and k_0. See Table 3. The Avrami-Erofeev indices n for the PE homopolymer and the PE_{50}-*b*-isotactic $PMMA_{50}$ diblock copolymer are 2.26 and 1.91, respectively. An index of $n = 1$ indicates one-dimensional linear growth (due to maximum impingement) while $n = 3$ means the typical three-dimensional spherical crystal growth (due to reduction of impingement). In our study, each index value is greater than one. Therefore, the crystallization derives structure formation and does not occur under absolute impinged conditions.[12] However, the degree of impingement is mildly more in the diblock copolymer than in the PE homopolymer. This finding may be attributed to adding the polar functional isotactic PMMA soft segment to the growing PE backbone (hard segment). Based on the values of n, the crystal growth (with respect to PE) in both polymers may be approximated to be mostly cylindrical. The postcrystallization morphology of a PE (semicrystalline)$_{26}$-*b*-polystyrene$_{74}$ (glassy amorphous) diblock copolymer, determined by transmission electron microscopy (TEM) supports our model-predicted morphology.[45,74] However, it should be noted that the variation in degree of cooling, segregation strength, and volume fraction of PE varies the postcrystallization morphology.

E_a of the copolymer crystallization (31.28 KJ/mol) is less than that of the homopolymer crystallization (37.29 KJ/mol).

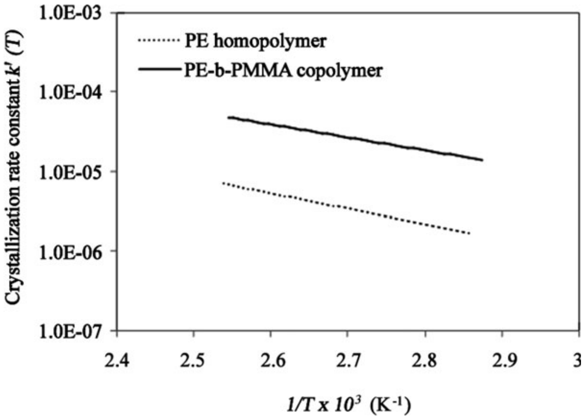

Figure 6. Model-predicted Arrhenius form of crystallization rate constant (Eq. 6) for PE homopolymer and PE-*b*-isotactic diblock copolymer.

For either polymer, E_a does not depend on relative crystallinity α. It remains constant as the crystallization proceeds. We previously defined $E_a = (E_{grow} - E_{nucl})$ that includes the energies needed to activate nucleation as well as crystal growth. Accordingly, $(E_{grow} - E_{nucl})|_{\text{PE-}b\text{-PMMA}} < (E_{grow} - E_{nucl})|_{\text{PE homopolymer}}$. The difference in E_a values can be attributed to the difference in the structural defect of the polymer backbones. The PE homopolymer is fairly linear whereas the copolymer has PMMA block with the pendant acrylate group ($-COOCH_3$) that can be considered as a kind of branch (Figure 2); hence, the copolymer has a constitutional structural defect.[75,76] Therefore, it requires less activation energy to crystallize.

The converse holds for the crystallization frequency factor $k_0 = \left[\frac{K_s N_0}{V_0}\right] \frac{k_{grow,0}}{k_{nucl,0}}$. The copolymer k_0 (0.699 s^{-1}) is slightly greater than that of the homopolymer (0.624 s^{-1}). See Table 2. The bulk crystallization rate of the copolymer (2.93×10^{-2} s^{-1}) differs from that of the homopolymer (2.62×10^{-2} s^{-1}) in an analogous fashion. These were calculated from the reciprocal of the half crystallization time $t_{1/2}$. The mutual variation of k_0 and $t_{1/2}^{-1}$, in each case, is about 12%. Therefore, the effects of the constitutional structural defect, due to the PMMA block, on k_0 and $t_{1/2}^{-1}$ may be considered negligible. This also indicates that $k_0|_{\text{PE-}b\text{-PMMA}}$ is comparable with $k_0|_{\text{PE homopolymer}}$ because of similar bulk

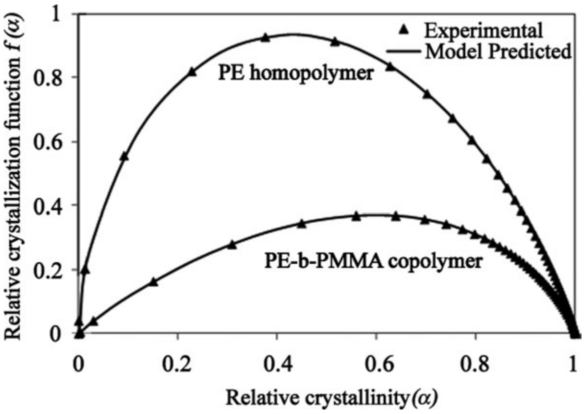

Figure 7. Variation of nonisothermal relative crystallization function $f(\alpha(T))$ as a function of relative crystallinity $\alpha(T)$.

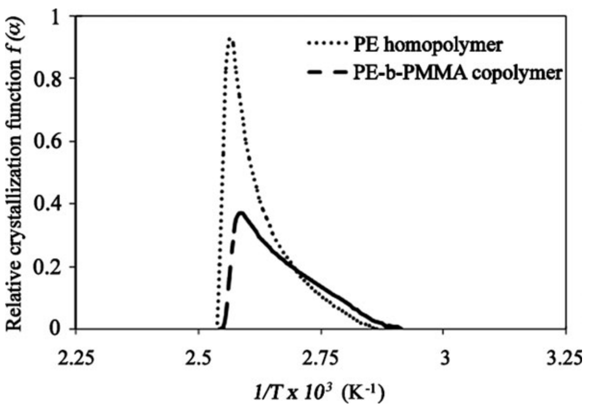

Figure 8. Effect of DSC cooling temperature on nonisothermal relative crystallization function $f(\alpha(T))$.

crystallization rates. In other words, the frequency of the occurrence of equilibrium chain folding that causes crystallization is similar in both polymers.[11,77]

Figure 7 shows how the nonisothermal relative crystallization function $f(\alpha)$ varied as a function of relative crystallinity α. Note that $f(\alpha)$ can be physically interpreted as the nonisothermal crystallization rate normalized with respect to the corresponding crystallization rate constant k' (T). See Eq. 8. The common observation is that for each polymer, the shape of $f(\alpha)$ is convex upward. This implies that the same crystallization mechanism prevails for both polymers all through the crystallization process. Also, there exists a relative crystallinity value $\alpha_{\max}$, corresponding to which $f(\alpha)$ shows a maximum. However, the features that differ are as follows:

- The $f(\alpha)$ profile for the block copolymer is skewed toward the right whereas that for the homopolymer, toward the left. In parallel, the former is significantly lower than the latter.
- $\alpha_{\max}|_{\text{PE homopolymer}} = 0.41$ $(n = 2.26)$, and $\alpha_{\max}|_{\text{PE-}b\text{-PMMA}} = 0.64$ $(n = 1.91)$, which shows that the maximum normalized crystallization rate occurs much earlier for the PE homopolymer than for the block copolymer. The corresponding α values calculated for an isothermal Avrami-Erofeev crystallization process (using Equation B20) are 0.33 and 0.43, respectively.
- The maximum of $f(\alpha)$ is positioned by $\alpha_{\max}$, and this depends on crystal growth dimension n; $\alpha_{\max}$ increased with the decrease in n. The literature supports this finding.[78]

The above results demonstrate the significant effect of the constitutional structural defect, introduced by the acrylate branch ($-COOCH_3$) of the isotactic polymethacrylate (PMMA) block (Figure 2) to the linear PE block, during crystallization. This effect is reflected in the normalized nonisothermal crystallization rate $f(\alpha)$ and the crystal growth dimension n.

Figure 8 illustrates how the DSC cooling temperature affected the nonisothermal relative crystallization function $f(\alpha)$. Each polymer shows similar variation pattern—a sharp rise in $f(\alpha)$ following a gradual decline—as the crystallization temperature continued to drop. This finding reaffirms the earlier statement that the same crystallization mechanism holds for both polymers all through the crystallization process. The temperature at which each curve shows a maximum is comparable. The maximum $f(\alpha)$ temperatures $T_{\max}$s for the homopolymer and the copolymer are 117.0°C ($\alpha_{\max}|_{\text{PE homopolymer}} = 0.41$, $\frac{E_a}{RT_{\max}} = 11.50$) and 114.0°C ($\alpha_{\max}|_{\text{PE-}b\text{-PMMA}} = 0.64$, $\frac{E_a}{RT_{\max}} = 10.54$), respectively. These $T_{\max}$ values are very near to the corresponding peak crystallization temperatures T_{pc}s (116.4 and 115.9°C). See Table 1. The closeness of these peak crystallization temperatures reflects minimal dilution effect by the PMMA block, which is associated with the poor miscibility of the amorphous block with the crystalline one.[45,74]

Postcrystallization polymer properties

Here, we discuss the postcrystallization polymer properties in terms of the following:

- lamellar thickness distribution (a nanoscopic property); and
- heat of fusion ΔH_f and peak melting temperature T_{mp} (bulk properties).

Figure 9 compares the lamellar thickness distribution in the PE homopolymer with that in the PE_{50}-*b*-$PMMA_{50}$ diblock copolymer. We calculated this property by applying Eqs. B2 and B3; and considering $T_m^0 = 145.5$ C, $\Delta H_f^0 = 290$ J/cm^3, and $\sigma_{\text{ssfe}} = 90$ mJ m^{-2}, which have been reported to be the best values to be used in the literature.[28] Further, for both polymers, these parameters, including σ_{ssfe} (crystallite specific surface free energy), were assumed to be the same. They fairly resemble each other; however, the distribution for the diblock copolymer is shifted toward the left. This means that the topological constraint imparted by the PMMA block mildly decreased the fraction of thicker lamellae. Also, the most probable lamellar thickness reduced from 9.45 to 9.12 nm. See Table 1.

The heat of fusion ΔH_f of the PE_{50}-*b*-$PMMA_{50}$ diblock copolymer (213.94 J/g, calculated on the basis of crystallizable PE block) is comparable with that of the PE homopolymer (214.8 J/g). However, ΔH_f of the PE_{50}-*b*-$PMMA_{50}$ diblock copolymer (108.20 J/g, calculated on the basis of the total mass of the copolymer) is significantly less than that of the PE homopolymer. This difference in ΔH_f also reflects the effect of the constitutional structural defect, introduced by the acrylate branch ($-COOCH_3$) of the (glassy/amorphous) isotactic polymethacrylate (PMMA) block (Figure 2) to the linear PE block, during crystallization.[75,76] This structural defect, on the contrary, did not practically affect the peak melting temperatures ($T_{mp}|_{\text{PE homopolymer}} = 132.4$°C, and $T_{mp}|_{\text{PE-}b\text{-PMMA}} = 131.2$°C). The latter finding—

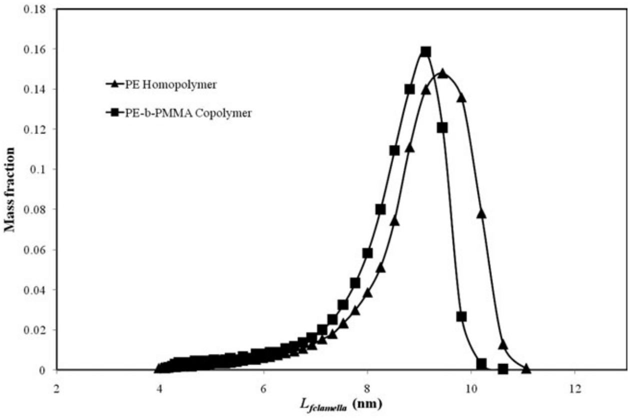

Figure 9. Comparison of postcrystallization lamellar thickness distribution in the PE homopolymer vs. PE-*b*-PMMA diblock copolymer.

inappreciable depression in melting point (~1°C)—indicates the formation of a continuous or percolated phase by the PE block.[45,74]

Conclusions

The crystallization behavior of PE-PMMA block copolymer significantly influences its morphology, thermal properties, and interfacial applications. Hence, we synthesized PE-*b*-isotactic PMMA diblock copolymer (through a sequential protocol), PE homopolymer, and isotactic PMMA using $SiMe_2(Ind)_2ZrMe_2$ and the MAO cocatalyst. We schematically explained the concerned polymerization mechanisms and the isotacticity of PMMA considering the relevant cationic catalytic species.

We used the above PE homopolymer and block copolymer to broaden the fundamental understanding of PE crystallization. For this purpose, we developed the appropriate nonisothermal Avrami-Erofeev crystallization model using a set of phenomenological assumptions. For each case, the model-predicted relative crystallinity profile matched well the entire DSC crystallinity profile, notably for a single value of the Avrami-Erofeev index n. Therefore, the developed nonisothermal crystallization model particularly overcomes the limitations of the existing nonisothermal crystallization models. This is a major contribution of this study. We compared the model-predicted crystallization parameters—n, apparent activation energy E_a, and crystallization frequency factor k_0—for both PE polymers. Based on the values of n (2.26 and 1.91), the crystal growth (with respect to PE) in both polymers may be approximated to be mostly cylindrical, which is supported by literature-reported TEM microgram.[45,74] The n values, being greater than one, indicate that the crystallization derives structure formation and does not occur under absolute impinged conditions.

The addition of the isotactic PMMA block to the linear PE block did not appreciably affect n, k_0, and bulk crystallization rate $t_{1/2}^{-1}$; and moderately influenced E_a. However, the constitutional structural defect, introduced by the acrylate branch ($-COOCH_3$) of the PMMA block, significantly influenced the heats of crystallization and fusion (ΔH_c and ΔH_f), %crystallinity, the nonisothermal crystallization rate constant k' (T), and the relative crystallization function $f(\alpha)$. ΔH_c, ΔH_f, %crystallinity, and $f(\alpha)$ were much less for the copolymer than for the PE homopolymer. However, the following thermal properties—peak crystallization point T_{pc}, peak melting point T_{mp}, the temperature for maximum nonisothermal relative crystallinity function T_{max}—were not greatly affected. We explained the physical significance of n, E_a, k_0, $t_{1/2}^{-1}$, and $f(\alpha)$ that provides interesting insight into PE crystallization. The closeness of crystallization temperatures reflects minimal dilution effect by the PMMA block whereas the inappreciable depression in melting point indicates the formation of a continuous or percolated phase by the PE block. The leftward shift of the lamellar thickness distribution of the diblock copolymer means that the topological constraint imparted by the PMMA block mildly decreased the fraction of thicker lamellae. The present study demonstrates how to correlate catalyst structure, functional block tacticity, and nonisothermal polyolefin crystallization and melting behavior.

Acknowledgments

The authors would like to acknowledge the support provided by the King Abdullah University of Science & Technology (KAUST) Center-in-Development for Transformative Research in Petrochemicals and Polymers at King Fahd University of Petroleum & Minerals (KFUPM), Dhahran, Saudi Arabia; as well as that, by King Abdulaziz City for Science and Technology (KACST) via the Science & Technology Unit at KFUPM through Project Number 08-PET90-4 as part of the National Science and Technology Innovation Plan. The technical assistance provided by the Center of Refining & Petrochemicals (CRP) of KFUPM Research Institute, the Center of Research Excellence in Petroleum Refining & Petrochemicals (CoRE-PRP) of KFUPM, and the Department of Chemical Engineering of KFUPM is also gratefully acknowledged. Special thanks are due to Prof. Asrof Ali, Department of Chemistry at KFUPM, for his useful technical discussions.

Literature Cited

1. Atiqullah M, Tinkl M, Pfaendner R, Akhtar MN, Hussain I. Synthesis of functional polyolefins using metallocenes: a comprehensive review. *Polym Rev*. 2010;50:178–230.
2. Atiqullah M, Akhtar MN, Tinkl M, Ahmed N. The role of allylanisole in metallocene-catalyzed propylene polymerization and synthesis of end-capped oligomers. *Macromol React Eng*. 2008;2:334–338.
3. Patil AO. Functional polyolefins. *Chem Innov*. 2000;30:19–24.
4. Aggarwal SL. *Block Copolymers*. New York: Plenum Press, 1970.
5. Riess G, Periard J, Bandereet A. *Colloidal and Morphological Behavior of Block and Graft Copolymers*. New York: Plenum Press, 1971.
6. Lohse D, Datta S, Kresge E. Graft copolymer compatibilizers for blends of polypropylene and ethylene-propylene copolymers. *Macromolecules*. 1991;24:561–566.
7. Kobori Y, Akiba I, Akiyama S. Compatibilizing effects of poly(ethylene-block-methyl methacrylate) on blends of polyethylene and poly(4-vinylphenol). *Polymer*. 2000;41:5971–5975.
8. Yasuda H, Furo M, Yamamoto H, Nakamura A, Miyake S, Kibino N. New approach to block copolymerizations of ethylene with alkyl methacrylates and lactones by unique catalysis with organolanthanide complexes. *Macromolecules*. 1992;25:5115–5116.
9. Domski GJ, Rose JM, Coates GW, Bolig AD, Brookhart M. Living alkene polymerization: new methods for the precision synthesis of polyolefins. *Prog Polym Sci*. 2007;32:30–92.
10. Hamley IW. Crystallization in block copolymers. *Adv Polym Sci*. 1999;148:114–137.
11. Hamley IW. *Developments in Block Copolymer Science and Technology*. New York: Wiley, 2004.
12. Müller AJ, Balsamo V, Arnal ML. Nucleation and crystallization in diblock and triblock copolymers. *Adv Polym Sci*. 2005;190:1–63.
13. Banks W, Hay JN, Sharples A, Thomson G. The crystallization of polyethylene II. *Polymer*. 1964;5:163–175.
14. Joshi M, Butola BS. Isothermal crystallisation of HDPE/POSS nanocomposite: effect of POSS as nanofiller. *J Appl Polym Sci*. 2007;105:978–985.
15. Vega JF, Martinez-Salazar J, Trujillo M, Arnal ML, Müller AJ, Bredeau S, Dubois Ph. Rheology, processing, tensile properties, and crystallization of polyethylene/carbon nanotube nanocomposites. *Macromolecules*. 2009;42:4719–4727.
16. Trakarnpruk W, Kajornkiratikul P, Praserthdam P. Polymerization of methylmethacrylate with zirconocene catalyst. *ACGC Chem Res Commun*. 2002;15:52–63.
17. Soga K, Deng H, Yano T, Shiono T. Stereospecific polymerization of methyl methacrylate initiated by dimethylzirconocene/$B(C_6F_5)_3$ (or $Ph_3CB(C_6F_5)_4$)/$Zn(C_2H_5)_2$. *Macromolecules*. 1994;27:7938–7940.
18. Balsamo V, Urdaneta N, Perez L, Carrizales P, Abetz V, Muller AJ. Effect of the polyethylene confinement and topology on its crystallisation within semicrystalline ABC triblock copolymers. *Eur Polym J*. 2004;40:1033–1049.
19. Graydon JW, Thorpe SJ, Kirk DW. Determination of the Avrami exponent for solid state transformations from nonisothermal differential scanning calorimetry. *J Non-Cryst Solids*. 1994;175:31–43.
20. Henderson DWJ. Experimental analysis of non-isothermal transformations involving nucleation and growth. *J Therm Anal*. 1979;15:325–331.
21. Ozawa, T. Kinetics of non-isothermal crystallization. *Polymer*. 1971;12:150–158.
22. Ruitenberg G, Woldt E, Petford-Long AK. Comparing the Johnson-Mehl-Avrami-Kolmogorov equations for isothermal and linear heating conditions. *Thermochim Acta*. 2001;378:97–105.
23. Jeziorny A. Parameters characterizing the kinetics of the nonisothermal crystallization of poly(ethylene terephthalate) determined by DSC. *Polymer*. 1978;19:1142–1144.

24. Liu TX, Mo ZS, Wang SG, Zhang HF. Nonisothermal melt and cold crystallization kinetics of poly(aryl ether ether ketone ketone). *Polym Eng Sci*. 1997;37:568–575.
25. Frauenrath H, Balk S, Keul H, Höcker H. First synthesis of an AB block copolymer with polyethylene and poly(methylmethacrylate) blocks using a zirconocene catalyst. *Macromol Rapid Commun*. 2001;22:1147–1151.
26. Jin J, Chen Y-XE. Stereoblock copolymerization of propylene and methyl methacrylate with single-site metallocene catalysts. *Macromol Chem Phys*. 2002;203:2329–2333.
27. Gedde UW. *Polymer Physics*. London: Chapman and Hall, 1995.
28. Zhou H, Wilkes GL. Comparison of lamellar thickness and its distribution determined from DSC, SAXS, TEM and AFM for high-density polyethylene films having a stacked lamellar morphology. *Polymer*. 1997;38:5735–5747.
29. Lu L, Alamo RG, Mandelkern L. Lamellar thickness distribution in linear polyethylene and ethylene copolymers. *Macromolecules*. 1994;27:6571–6576.
30. Pereira RA, Mano EB, Dias ML, Acordi EB. Comparative study on the lamellar crystal structure of high- and low-density polyethylenes. *Polym Bull. (Berlin)* 1997;38:707–714.
31. Islam MA, Hussein IA, Atiqullah M. Effects of branching characteristics and copolymer composition distribution on non-isothermal crystallization kinetics of metallocene LLDPEs. *Eur Polym J*. 2007;43:599–610.
32. Hussain I, Atiqullah M, Fazal A, Alam K, Hossaen A. Effect of selected residual Ziegler-Natta and metallocene catalysts on the UV-induced degradation of unstabilized ethylene homopolymer films. *Polym Degrad Stab*. 2010;95:2289–2299.
33. Wood-Adams PM, Dealy JM, deGroot AW, Redwine OD. Effect of molecular structure on the linear viscoelastic behavior of polyethylene. *Macromolecules*. 2000;33:7489–7499.
34. Krüger P. On the relation between nonisothermal and isothermal Kolmogorov-Johnson-Mehl-Avarmi crystallization kinetics. *J Phys Chem Solids*. 1993;54:1549–1555.
35. Kanervo J, Krause AOI. Kinetic analysis of temperature-programmed reduction: behavior of a CrOx/Al2O3 catalyst. *J Phys Chem B*. 2001;105:9778–9784.
36. Cao J. Re-examination of a proposed method to obtain Avrami parameters directly from non-isothermal crystallization data. *Polymer*. 1992;33:3520–3521.
37. Málek J. The applicability of Johnson-Mehl-Avrami model in the thermal analysis of the crystallization kinetics of glasses. *Thermochim Acta*. 1995;267:61–73.
38. Farjas J, Roura P. Modification of the Kolmogorov–Johnson–Mehl–Avrami rate equation for non-isothermal experiments and its analytical solution. *Acta Mater*. 2006;54:5573–5579.
39. Va'zquez J, Lo'pez-Alemany PL, Villares P, Jime'nez-Garay R. Generalization of the Avrami equation for the analysis of non-isothermal transformation kinetics. Application to the crystallization of the Cu0.20As0.30Se0.50 alloy. *J Phys Chem Solids*. 2000;61:493–500.
40. Routray K, Deo G. Kinetic parameter estimation for a multi-response nonlinear reaction model. *AIChE J*. 2005;51:1733–1746.
41. Fogler HS. *Elements of Chemical Reaction Engineering*, 4th ed. New Jersey: Prentice Hall International, 2006.
42. Hossain MM, de Lasa HI. Reactivity and stability of Co-Ni/Al_2O_3 oxygen carrier in multicycle CLC. *AIChE J*. 2007;53:1817–1829.
43. Watts DG. Estimating parameters in nonlinear rate equations. *Can J Chem Eng*. 1994;72:701–710.
44. Kanervo J, Krause AOI. Characterisation of supported chromium oxide catalysts by kinetic analysis of H_2-TPR data. *J Catal*. 2002;207:57–65.
45. Lorenzo AT, Arnal ML, Müller AJ, Albuerne J. DSC isothermal polymer crystallization kinetics measurements and the use of the Avrami equation to fit the data: Gudielines to avoid common problems. *J Polym Test*. 2007;26:222–231.
46. Órfáo JJM. Review and evaluation of the approximations to the temperature integral. *AIChE J*. 2007;53:2905–2915.
47. Deng C, Cai J, Liu R. Kinetic analysis of solid-state reactions: evaluation of approximations to temperature integral and their applications. *Solid State Sci*. 2009;11:1375–1379.
48. Brar AS, Singh G, Shankar R. Structural investigations of poly(methyl methacrylate) by two-dimensional NMR. *J Mol Struct*. 2004;703:69–81.
49. Atiqullah M, Nauman EB. A model and measurement technique for micromixing in copolymerization reactors. *Chem Eng Sci*. 1990;45:1267–1279.
50. Atiqullah M, Hassan MM, Beg SA. Modeling the effects of micromixing and start-up procedures on bulk copolymerization and copolymer in a tubular reactor. *J Appl Polym Sci*. 1992;46:879–889.
51. Atiqullah M. Imperfect/incomplete micromixing effects on copolymerization in a premixed-feed stirred tank reactor. *Eur Polym J*. 1993;29:1581–1588.
52. Monrabal B. Crystallization analysis fractionation: a new technique for the analysis of branching distribution in polyolefins. *J Appl Polym Sci*. 1994;52:491–499.
53. Soares JBP, Monrabal B, Nieto J, Blanco J. CRYSTAF analysis of poly(ethylene-co-1-octene) made with single site type catalysts: a mathematical model for the dependence of composition distribution on molecular weight. *Macromol Chem Phys*. 1998;199:1917–1926.
54. Beigzadeh D, Soares JBP, Duever TA. Modelling of CRYSTAF fractionation using Monte Carlo simulation of crystallizable sequence lengths: ethylene-1-octene copolymers synthesized with single-site-type catalysts. *J. Appl Polym Sci*. 2001;80:2200–2206.
55. Simon LC, Patel H, Soares JBP, de Souza RF. Polyethylene made with in-situ supported Ni-diimine/SMAO: replication phenomenon and effect of polymerization conditions on polymer microstructure and morphology. *Macromol Chem Phys* 2001;202:3237–3247.
56. Chen EYX, Marks T J. Cocatalysts for metal-catalyzed olefin polymerization: activators, activation processes, and structure−activity relationships. *Chem Rev*. 2000;100:1391–1434.
57. Atiqullah M, Faiz M, Akhtar MN, Salim MA, Ahmed S, Khan JH. XPS investigation of the electronic environment in selected heterogenized zirconocene catalysts. *Surf Interface Anal*. 1999;27:728–734.
58. Atiqullah M, Akhtar MN, Faiz M, Moman A, Abu-Raqabah AH, Khan JH, Wazeer M I. Surface chemistry of selected supported metallocene catalysts studied by DR-FTIR, CPMAS NMR, and XPS techniques. *Surf Interface Anal*. 2006;38:1319–1327.
59. Atiqullah M. *Heterogeneous olefin polymerization metallocene catalysts: the application and role of group 14 lewis acid silica support modifiers*. In: Marmaduke, DL, editor. *Progress in Heterogeneous Catalysis*. New York: Nova Science, 2008.
60. Belelli PG, Branda MM, Castellani NJ. DFT studies of zirconocene/MAO interaction. *J Mol Catal A: Chem*. 2003;192:9–24.
61. Chien JCW, He DJ. Olefin copolymerization with metallocene catalysts. III. Supported metallocene/methylaluminoxane catalyst for olefin copolymerization. *J Polym Sci Part A: Polym Chem*. 1991;29:1603–1607.
62. Soga K, Kaminaka M. Copolymerization of olefins with SiO_2-, Al_2O_3-, and $MgCl_2$-supported metallocene catalysts activated by trialkylaluminiums. *Macromol Chem Phys*. 1994;195:1369–1379.
63. Ciardelli F, Altomare A, Michelotti M. From homogeneous to supported metallocene catalysts. *Catal Today*. 1998;41:149–157.
64. Frauenrath H, Keul H, Höcker H. Stereospecific polymerization of methyl methacrylate with single-component zirconocene complexes: Control of stereospecificity via catalyst symmetry. *Macromolecules*. 2001;34:14–19.
65. Delgado AR, Chen Y-XE. Mechanistic studies of stereospecific polymerization of methacrylates using a cationic, chiral ansa-zirconocene ester enolate. *Macromolcules*. 2005;38:2587–2594.
66. Cossee P. Mechanism of polymerization of α-olefins with Ziegler-Natta catalysts. *J Catal*. 1964;3:80–88.
67. Arlman EJ, Cossee P. Ziegler-Natta catalysis III. Stereospecific polymerization of propene with the catalyst system $TiCl_3$-$AlEt_3$. *J Catal*. 1964;3:99–104.
68. Hossain MM, de Lasa HI. Reduction and oxidation kinetics of Co-Ni/Al_2O_3 oxygen carrier involved in a chemical looping combustion process. *Chem Eng Sci*. 2010;65:98–106.
69. Zhang C, Wu HF, Ma CA, Sumita M. Effect of vapor grown carbon fiber on non-isothermal crystallization kinetics of HDPE/PMMA blend. *Mater Lett*. 2006;60:1054–1058.
70. Acar I, Durmuş A, Özgümüş S. Nonisothermal crystallization kinetics and morphology of poly(ethylene terephthalate) modified with poly(lactic acid). *J Appl Polym Sci*. 2007;106:4180–4191.
71. Olmos D, Dominguez C, Castrillo PD, Gonzalez-Benito. Crystallization and final morphology of HDPE: effect of the high energy ball milling and the presence of TiO_2 nanoparticles. *Polymer*. 2009;50:1732–1742.
72. Papageorgiou G, Bikiaris DN, Chrissafis K. A different approach for the study of the crystallization kinetics in polymers. Key study: poly(ethylene terephthalate)/SiO_2 nanocomposites. *Polym Int*. 2010;59:1630–1638.
73. Adhikari A, Lozano K. Effects of carbon nanofibers on the crystallization kinetics of polyethylene oxide. *J Polym Res*. 2011;18:875–880.
74. Lorenzo AT, Arnal ML, Muller AJ, Boschetti-de-Fierro A, Abetz V. Nucleation and isothermal crystallization of the polyethylene block

within diblock copolymers containing polystyrene and poly(ethylene-alt-propylene). *Macromolecules*. 2007;40:5023–5037.

75. Martuscelli E, Pracella M. Effects of chain defects on the thermal behavior of polyethylene. *Polymer*. 1974;15:306–314.
76. Risch BG, Wilkes GL, Warakomski JM. Crystallization kinetics and morphological features of star-branched nylon-6: effect of branch-point functionality. *Polymer*. 1993;34:2330–2343.
77. Galwey AK, Brown ME. Arrhenius parameters and compensation behavior in solid-state decompositions. *Thermochim Acta*. 1997;300:107–115.
78. Vyazovkin S, Burnham AK, Criado JM, Pérez-Maqueda LA, Popescu C, Sbirrazzuoli N. ICTAC Kinetics Committee recommendations for performing kinetic computations on thermal analysis data. *Thermochim Acta*. 2011;520:1–29.
79. Avrami M. Kinetics of phase change. I. *J Chem Phys*. 1939;7:1103–1112.
80. Avrami M. Kinetics of phase change. II. *J Chem Phys*. 1940;8:212–224.
81. Avrami M. Kinetics of phase change. III. *J Chem Phys*. 1941;9:177–184.
82. Brown WE, Dollimore D, Galwey AK. *Reaction in the solid state*. In: Bamford CH, Tipper CFH, editors. *Comprehensive Reaction Kinetics*. Amsterdam: Elsevier Scientific Publishing Company, Part 22, 1980; 49–59.
83. Cahn JW. The dependence of grain-boundary precipitation rates on the orientation of adjoining grains. *Acta Mater*. 1956;4:449–459.
84. Erofeyev BVCR. Generalized equation of chemical kinetics and its application in reactions involving solids. *Compt Rend Acad Sci URSS*. 1946;52:511–514.

Appendix A: Derivation of Relative Crystallinity Function *f(α)* and Isothermal Avrami-Erofeev Crystallization Rate Equation

The relative crystallinity function $f(\alpha)$ can be derived in the form of Avrami-Erofeev model by considering the following:[79–82]

- formation of crystal nuclei at time τ (that occupies a volume $V(t, \tau)$ at time t);
- rate of crystal nuclei growth represented by $\left(\frac{dN}{dt}\right)_{t=\tau}$; and
- the occurrence of randomly distributed nuclei (crystal morphology).

As per the above constitutive framework, the total volume of material $V_{\text{total}}(t)$, that crystallizes from a given molten polymer mass, can be expressed by the following equation[35,42,82]

$$V_{\text{total}}(t) = \int_0^t V(t,\tau) \left(\frac{dN}{dt}\right)_{t=\tau} d\tau \tag{A1}$$

Equation A1 is fundamentally a general convolution integral that comprises a rate law of nucleation $\left(\frac{dN}{dt}\right)_{t=\tau}$, and a formalism for nuclei growth $V(t, \tau)$. In this regard, N denotes the number of active (growing) nuclei and $V(t, \tau)$ gives the volume at time t for a nucleus that became activated at time τ. In principle, Eq. A1 describes a class of models with different nucleation and growth processes.

First, we shall consider $\left(\frac{dN}{dt}\right)_{t=\tau}$. In the literature, several nucleation rate laws, such as first-order, instantaneous, linear, random (with unimolar decay), etc. are available.[44,82] In this particular situation, we apply the first-order nucleation. This means that the rate of nucleation is linearly related to the difference between the number of germ nuclei N_0 (the potential nucleus formation sites/defects) and the number of growing (active) nuclei N as follows

$$\left(\frac{dN}{dt}\right)_{t=\tau} = k_{\text{nucl}}(N_0 - N) \tag{A2}$$

where k_{nucl} is the first-order nucleation rate constant. Integration of Eq. A2 with $N = 0$ for $t = 0$ gives

$$N = N_0\left[1 - e^{(-k_{\text{nucl}}\tau)}\right] \tag{A3}$$

Differentiation of Eq. A3 with respect to t leads to the following exponential law of nucleation

$$\left(\frac{dN}{dt}\right)_{t=\tau} = k_{\text{nucl}} N_0 e^{(-k_{\text{nucl}}\tau)} \tag{A4}$$

We may note the following from Eq. A4. When k_{nucl} is large, nucleation is virtually instantaneous, $N = N_0$; and no further nuclei are generated during subsequent cooling of the molten polymer. On the other hand, when k_{nucl} is small, the rate of nucleation is approximately constant because the number of sites (N_0–N) changes little. This is known as the linear law of nucleation

$$N = k_{\text{nucl}}\, N_0\, t \tag{A5}$$

Now, we shall derive a formalism for $V(t, \tau)$. In this connection, we assume that the radius of nucleus $r(t, \tau)$ increases with a rate $k_{\text{grow}}(t*)$ as follows[35]

$$r(t,\tau) = \int_\tau^t k_{\text{grow}}(t*)dt* \tag{A6}$$

For n-dimensional isotropic nuclei growth, $V(t, \tau)$ can be expressed as[35]

$$V(t,\tau) = K_{\text{s}}[r(t,\tau)]^{\,n} = K_{\text{s}}\left[\int_\tau^t k_{\text{grow}}(t*)dt*\right]^{\,n} \tag{A7}$$

where K_{s} is the shape factor for the growing nuclei.

Substitution of Eqs. A7 and A4 into Eq. A1 yields

$$V_{\text{total}}(t) = \int_0^t K_{\text{s}}\left[\int_\tau^t k_{\text{grow}}(t*)dt*\right]^{\,n} k_{\text{nucl}} N_0 e^{-k_{\text{nucl}}\tau} d\tau \tag{A8}$$

Equation A8 applies to any type of thermal history. Let us assume that $k_{\text{grow}}\,(t^*) \neq f(t^*)$, and consider an isothermal case; then, k_{grow} represents a time-invariant nucleation growth constant. Under these two conditions, Eq. A8 becomes

$$V_{\text{total}}(t) = \int_0^t K_{\text{s}}\left[k_{\text{grow}} \times (t-\tau)\right]^{\,n} k_{\text{nucl}} N_0 e^{-k_{\text{nucl}}\tau} d\tau \tag{A9}$$

The analytical solution of Eq. A9, following successive integration by parts, can be written as

$$V_{\text{total}}(t) = \frac{K_{\text{s}} N_0 k_{\text{grow}}^n n!}{k_{\text{nucl}}^n}(-1)^{\,n+1}\left[e^{-k_{\text{nucl}}t} - \sum_{i=0}^{n}(-1)^{\,i}\frac{(k_{\text{nucl}}t)^{\,i}}{i!}\right] \tag{A10}$$

Division of both sides of Eq. A10 by the initial volume of the molten polymer V_0, yields the extended relative crystallinity $\alpha_{\text{ex}}(t)$ as follows

$$\alpha_{\mathrm{ex}}(t) = \frac{V_{\mathrm{total}}(t)}{V_0} = \frac{K_{\mathrm{s}} N_0 k_{\mathrm{grow}}^n n!}{V_0 k_{\mathrm{nucl}}^n} (-1)^{n+1} \left[e^{-k_{\mathrm{nucl}} t} - \sum_{i=0}^{n} (-1)^{i} \frac{(k_{\mathrm{nucl}} t)^{i}}{i!} \right] \tag{A11}$$

So far, the nuclei have been allowed to grow in an unlimited fashion (ignoring the constraints of overlap and site ingestion) as per the exponential law of nucleation, that is, Eq. A4. However, the growing nuclei will eventually reach the boundaries of the crystallizing polymer; the nuclei boundaries will overlap; and they may also ingest the germ nuclei. To account for these phenomena, $\alpha_{\mathrm{ex}}(t)$ is to be converted to the true relative crystallinity $\alpha(t)$ (fractional extent of crystallization), using the following relation proposed by Avrami for locally random distribution of germ nuclei[79–82]

$$d\alpha(t) = [1-\alpha(t)]\, d\alpha_{\mathrm{ex}}(t) \Leftrightarrow \alpha_{\mathrm{ex}}(t) = -\ln[1-\alpha(t)] \tag{A12}$$

Substitution of Eq. A12 into Eq. A11 gives

$$-\ln[1-\alpha(t)] = \frac{K_{\mathrm{s}} N_0 k_{\mathrm{grow}}^n n!}{V_0 k_{\mathrm{nucl}}^n} (-1)^{n+1} \left[e^{-k_{\mathrm{nucl}} t} - \sum_{i=0}^{n} (-1)^{i} \frac{(k_{\mathrm{nucl}} t)^{i}}{i!} \right] \tag{A13}$$

We have two time scales. One is the macroscopic time scale for the overall crystallization process, and the other is the microscopic time scale for nucleation. In practice, $t >> \tau$, that is, all nucleation is completed before crystal growth.[37] This represents a situation of site saturation.[20,83] Then, the right hand side of Eq. A13, for the limiting case of large k_{nucl} (high nucleation rate), can be approximated with the highest order term of the summation series, and using $e^{-k_{\mathrm{nucl}} t} \approx 0$. This reduces Eq. A13 to

$$-\ln(1-\alpha(t)) = \frac{K_{\mathrm{s}} N_0 k_{\mathrm{grow}}^n}{V_0 k_{\mathrm{nucl}}^n} t^n = (kt)^n \Leftrightarrow \alpha(t) = 1 - e^{-(kt)^n} \tag{A14}$$

where $k = \left[\frac{K_{\mathrm{s}} N_0}{V_0}\right]^{1/n} \frac{k_{\mathrm{grow}}}{k_{\mathrm{nucl}}}$ = overall crystallization rate constant.

Erofeev derived analogous material transformation expression from completely different considerations. Despite the conceptual difference, Erofeev's probabilistic approach inherently includes the same assumptions as Avrami's treatment.[84] Therefore, Eq. A14 is the well-known Avrami-Erofeev equation for isothermal crystallization, which yields the following relation

$$kt = [-\ln(1-\alpha(t))]^{\frac{1}{n}} \tag{A15}$$

Differentiation of Eq. 14 gives the following rate of crystallization

$$\frac{d\alpha}{dt} = nk^n t^{n-1} e^{-(kt)^n} \tag{A16}$$

The isothermal crystallization rate can also be expressed in terms of the relative crystallization function $f(\alpha(t))$ as follows

$$\frac{d\alpha}{dt} = kf(\alpha(t)) \tag{A17}$$

Equations A14–A16 can be combined to give the final isothermal Avrami-Erofeev relative crystallinity function

$$f(\alpha(t)) = n(1-\alpha(t))\,[-\ln(1-\alpha(t))]^{\frac{n-1}{n}} \tag{A18}$$

Therefore, the isothermal Avrami-Erofeev polymer crystallization rate can be written as

$$\frac{d\alpha(t)}{dt} = k \times n(1-\alpha(t))\,[-\ln(1-\alpha(t))]^{\frac{n-1}{n}} \tag{A19}$$

Equation A19 shows that for a given value of n, the isothermal polymer crystallization rate is a simple function of temperature (through k), and the volume fraction transformed.

Differentiating both sides of Eq. A18 with respect to $\alpha(t)$ and equating the same to zero, $\alpha_{\max}$ can be obtained in the form of the following expression

$$\alpha_{\max} = 1 - e^{\frac{1-n}{n}} \tag{A20}$$

where $\alpha_{\max}$, a function of only n, is the value of relative crystallinity corresponding to which the isothermal relative crystallinity function $f(\alpha(t))$ has a maximum.

Appendix B: Calculation of Lamellar Thickness Distribution using Constant Heating Rate DSC Experiment

PEs, including other members of polyolefins, are semicrystalline materials. Considering an orthogonal frame work, and chain-folding mechanism of crystallization, the melting point T_{m} and the corresponding dimensions of a crystal lamella (crystallite) can be thermodynamically related as follows through the traditional Gibbs-Thomson equation[27,28]

$$T_{\mathrm{m}} = T_{\mathrm{m}}^0 \left[1 - \left(\frac{\sigma_1}{L_1} + \frac{\sigma_2}{L_2} + \frac{\sigma_3}{L_3}\right) \frac{2}{\Delta H_{\mathrm{f}}^0}\right] \tag{B1}$$

where T_m^0 is the equilibrium melting temperature of a crystal of infinite thickness; σ_1, σ_2, and σ_3 are the basal specific surface free energies of the crystallite, and they are associated with the energy of chain folding during the crystallization process; L_1, L_2, and L_3 are the corresponding dimensions along the three orthogonal directions. ΔH_{f}^0 is the heat of fusion per unit volume for the crystalline phase (perfect crystallite). Now, let us assume the following:

- The lateral and transverse dimensions of the folded-chain crystallite in bulk are much larger than the lamellar thickness. This means that L_2 and $L_3 >> L_1$, which leads to $L_1 = L_{\mathrm{fclamella}}$ (folded crystal lamellar thickness), and $\sigma_1 = \sigma_{\mathrm{ssfe}}$ (crystallite specific surface free energy).
- Over the temperature range under consideration, the crystallite parameters do not depend on temperature T and lamellar thickness $L_{\mathrm{fclamella}}$.

Then Eq. B1 reduces to the following expression[28–30]

$$T_{\mathrm{m}} = T_{\mathrm{m}}^0 \left[1 - \frac{2\sigma_{\mathrm{ssfe}}}{\Delta H_{\mathrm{f}}^0 L_{\mathrm{fclamella}}}\right] \tag{B2}$$

Equation B2 shows that T_m decreases as $L_\mathrm{fclamella}$ decreases; the converse is also true; and $T_\mathrm{m} \rightarrow T_m^0$ as $L_\mathrm{fclamella} \rightarrow \infty$. Therefore, an asymptotic relation holds between T_m and $L_\mathrm{fclamella}$.

Now we shall show how to calculate the distributions of lamellar thickness and chain fold length, using a typical DSC endotherm. For this purpose, we assume that the rate of heat flow, at a given temperature, is proportional to the mass of a crystallite (having a lamellar thickness between $L_\mathrm{fclamella}$ and $L_\mathrm{fclamella} + dL_\mathrm{fclamella}$, that has melted during dT.[28,29] Accordingly, the melted crystallite mass fraction χ_i at time t_i and temperature T_i is given by

$$\chi_i(t) = \frac{\int_{t_0}^{t+dt} \left(\frac{dH}{dt}\right) dt|_{i+1} - \int_{t_0}^{t} \left(\frac{dH}{dt}\right) dt|_i}{\int_{t_0}^{t_\infty} \left(\frac{dH}{dt}\right) dt} \tag{B3}$$

Note that all the integrals in Eq. B3 is automatically generated as a function of time and temperature by the software of a standard computer-assisted DSC instrument.

Manuscript received Nov. 13, 2011, and revision received Mar. 17, 2012.